Geometric and Cognitive Differences between Logical Diagrams for the Boolean Algebra $\mathbb{B}_4$

Lorenz Demey and Hans Smessaert

Abstract

Aristotelian diagrams are used extensively in contemporary research in artificial intelligence. The present paper investigates the geometric and cognitive differences between two types of Aristotelian diagrams for the Boolean algebra $\mathbb{B}_4$. Within the class of 3D visualizations, the main geometric distinction is that between the cube-based diagrams (such as the rhombic dodecahedron) and the tetrahedron-based diagrams. Geometric properties such as collinearity, central symmetry and distance are examined from a cognitive perspective, focusing on diagram design principles such as congruence/isomorphism and apprehension. The cognitive effectiveness of the different visualizations is compared for the representation of implication versus opposition relations, and for subdiagram embeddings.

Keywords: logical geometry, knowledge representation, rhombic dodecahedron, tetrahedron, opposition and implication, congruence principle, central symmetry.

1 Introduction

The logical diagrams used in philosophy and artificial intelligence can be divided into two broad classes. On the one hand, there is the class containing, among others, Euler, Venn, spider and linear/interval diagrams [9, 40, 43, 65, 92]. In these cases, one diagram visualizes a *single formula* from a given logical system, and visual operations on the diagram correspond to logical operations on the formula. Diagrammatic reasoning thus consists in a sequence of operations that gradually transforms an initial diagram into another diagram. On the other hand, there is the class containing, for instance, Hasse, Aristotelian and duality diagrams [17, 24, 30, 82], where one diagram visualizes the logical relations between *several formulas* from a given logical system. Such diagrams support different types of inference, which consists in 'traversing' the diagram by making use of the relations

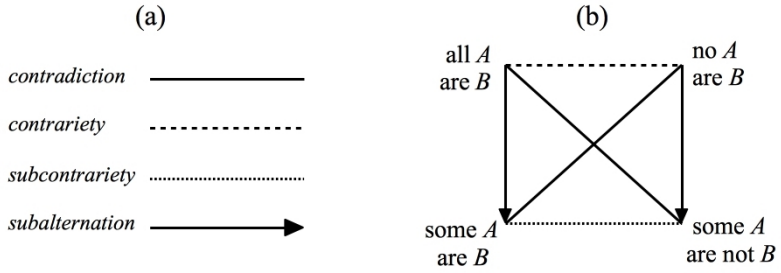

Figure 1: (a) Visual code for representing the Aristotelian relations, (b) square of opposition for the categorical statements.

between the formulas,[1] and thus resemble the proof technique of diagram chasing in category theory [5].[2]

In this paper we will focus on logical diagrams of the second class, and in particular, on Aristotelian diagrams. These diagrams visualize the Aristotelian relations holding between certain formulas, according to the visual code shown in Figure 1(a). A formal definition of the Aristotelian relations in terms of Boolean algebras will be introduced in Section 2. Without a doubt, the most well-known example of an Aristotelian diagram is the square of opposition for the categorical statements from syllogistics [67], as shown in Figure 1(b). Some examples of larger, more complex Aristotelian diagrams are shown in Figure 2. The octagon in Figure 2(b) was already studied by the 14th-century philosopher John Buridan [31, 52, 55, 76]. This clearly illustrates the fact that Aristotelian diagrams have a long and rich history in philosophy [20, 21, 67]. However, today they are also widely used in other areas, including artificial intelligence. For example, they have been used in the study of various logic-based approaches to knowledge representation, such as modal/epistemic logic [7, 18, 42, 57, 58], fuzzy logic [47, 62, 63, 64, 89], propositional dynamic logic [18, 44] and probabilistic logic [45, 70, 71, 79]. Furthermore, Aristotelian diagrams are also used extensively to study other types of knowledge representation formalisms, including rough set theory [13, 94, 14], formal concept analysis and possibility theory [14, 33, 34], formal

[1] For example, many logic textbooks targeted at philosophy students contain exercises in which one is presented with a square of opposition and the truth value of (the formula in) one of the square's corners, and is then asked to determine the truth values of the other corners by making use of the Aristotelian relations [53, Exercise 4.5.1].

[2] There also exists some overlap between these two classes of logical diagrams. For example, philosophers [6] and computer scientists [48] have recently developed diagrams where the individual formulas are visualized as small Euler/Venn diagrams, which are then embedded inside a larger Aristotelian/Hasse diagram.

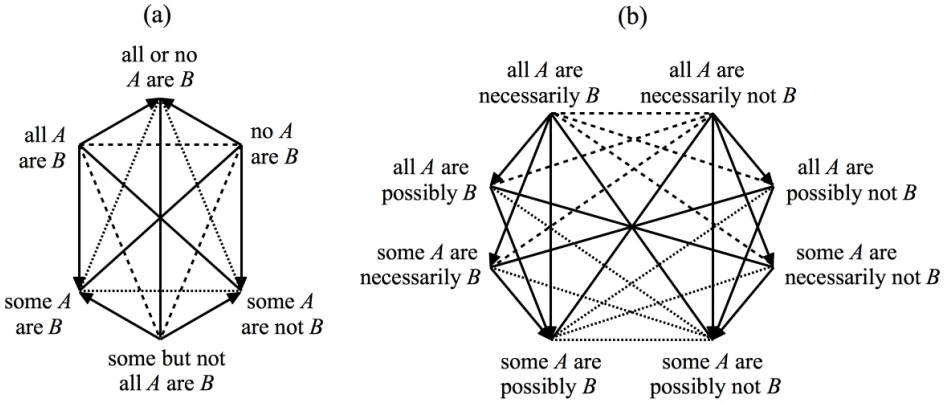

Figure 2: Two larger, more complex Aristotelian diagrams.

argumentation theory [1, 2, 3, 4], fuzzy set theory [15, 16, 35, 38], the theory of logical and analogical proportions [59, 72, 73, 74, 75] and multiple-criterion decision-making [36, 37, 39]. Dubois et al. [36] and Yao [94] present a general perspective on the usefulness of Aristotelian diagrams in the theoretical foundations of artificial intelligence, emphasizing their role in drawing comparisons across individual formalisms and in discovering new notions.

The research programme of Logical Geometry[3] studies Aristotelian diagrams from both an abstract-logical and a visual-geometrical perspective. The abstract-logical properties are analyzed using tools and techniques from model theory [29, 83], group theory [17, 26], combinatorics [25, 29], lattice theory [24, 80] and formal semantics [80, 84]. The study of visual-geometrical topics makes crucial use of insights from disciplines such as information visualization [19, 82], diagram design [27, 81] and cognitive psychology [25, 82]. One of the major visual-geometrical issues studied in Logical Geometry is the fact that a single logical structure often gives rise to different visualizations [25]. In particular, when drawing Aristotelian diagrams for a given logical structure, one is still confronted with several design choices. In Larkin and Simon's terminology [56], the resulting diagrams are *informationally* equivalent, but they need not be *computationally* equivalent, in the sense that visual differences may significantly influence user comprehension. Since authors typically use Aristotelian diagrams to help their readers gain a better insight into the underlying logical structures, the question arises whether some diagrams are more 'effective' than others.

The main aim of this paper is to present a case study on this question: we take

[3] See `www.logicalgeometry.org`.

one logical structure, viz. the Boolean algebra $\mathbb{B}_4$, and compare two fundamentally different 3D visualizations in the light of general principles of diagram design and information visualization. This case study is particularly interesting in the context of artificial intelligence, for a number of different (but interrelated) reasons. First of all, one of the visualizations to be studied was first proposed and analyzed by AI researchers, viz. Ciucci, Dubois and Prade [13, 33]. Furthermore, as is explicitly indicated by these authors, the Boolean algebra $\mathbb{B}_4$ naturally arises in the context of a *quadripartition* of a given set. In this sense we go one step beyond the Boolean algebra $\mathbb{B}_3$, which corresponds to a *tripartition*, and is typically visualized by means of a hexagon of opposition (also see related work on orthopairs and three-way decisions [11, 12, 94, 95]). Finally, the present case study strikes a good balance between logical complexity and geometrical simplicity: on the one hand the Boolean algebra $\mathbb{B}_4$ is sufficiently complex to be useful in actual AI applications (such as formal concept analysis), but on the other hand its 3D visualizations are still sufficiently simple to be readily accessible for human visual perception.[4]

The paper is organized as follows. Section 2 introduces the Boolean algebra $\mathbb{B}_4$, its canonical bitstring representation and the Aristotelian relations. Section 3 discusses the geometric differences between cube-based and tetrahedron-based 3D visualizations of $\mathbb{B}_4$, focusing on the rhombic dodecahedron and the nested tetrahedron. Sections 4 – 7 contain the core results of this paper, offering a detailed comparison of the cognitive effectiveness of the different 3D visualizations from the perspective of diagram design principles such as congruence/isomorphism and apprehension.[5] In particular, Section 4 studies the representation of implication relations and logical levels, whereas Section 5 deals with the visualization of the opposition relations of contradiction and (sub)contrariety. Next, Section 6 investigates a number of visualization issues that simultaneously involve implication and opposition. Section 7 studies how certain well-known subdiagrams, such as squares and hexagons, can be embedded inside the larger 3D diagrams. Finally, Section 8 offers some concluding remarks.

[4] One might point out that Dubois, Prade et al.'s 'cube of opposition' is also very useful in artificial intelligence [16, 36], and is visually even much simpler. However, unlike the diagrams studied in this paper, this cube is not Boolean closed: it does not visualize an entire Boolean algebra, but only a part of one. In [22] it is shown that the Boolean closure of this cube of opposition is (isomorphic to) $\mathbb{B}_7$, which contains $2^7 = 128$ elements, and thus cannot be visualized in an easily surveyable manner.

[5] Moretti [61] and Dubois and Prade [33] provide an initial comparison between the cube- and tetrahedron-based diagrams, but without focusing on diagram design principles. The outlines of a more cognitively oriented comparison are sketched in [85].

Table 1: Bitstrings for the 16 formulas of CPL and S5.

$\varphi \in \mathcal{L}_{\mathsf{S5}}$	$\psi \in \mathcal{L}_{\mathsf{CPL}}$	$\beta(\varphi)/\beta(\psi)$	$\beta(\neg\varphi)/\beta(\neg\psi)$	$\neg\psi \in \mathcal{L}_{\mathsf{CPL}}$	$\neg\varphi \in \mathcal{L}_{\mathsf{S5}}$
$\Box p$	$p \wedge q$	1000	0111	$\neg(p \wedge q)$	$\neg\Box p$
$p \wedge \neg\Box p$	$\neg(p \rightarrow q)$	0100	1011	$p \rightarrow q$	$\neg p \vee \Box p$
$\neg p \wedge \Diamond p$	$\neg(p \leftarrow q)$	0010	1101	$p \leftarrow q$	$p \vee \neg\Diamond p$
$\neg\Diamond p$	$\neg(p \vee q)$	0001	1110	$p \vee q$	$\Diamond p$
p	p	1100	0011	$\neg p$	$\neg p$
$\Box p \vee (\neg p \wedge \Diamond p)$	q	1010	0101	$\neg q$	$\neg\Box p \wedge (p \vee \neg\Diamond p)$
$\Box p \vee \neg\Diamond p$	$p \leftrightarrow q$	1001	0110	$\neg(p \leftrightarrow q)$	$\neg\Box p \wedge \Diamond p$
$\Box p \wedge \neg\Box p$	$p \wedge \neg p$	0000	1111	$p \vee \neg p$	$\Box p \vee \neg\Box p$

2 Bitstrings and Aristotelian Relations in $\mathbb{B}_4$

In its investigations, Logical Geometry makes extensive use of *bitstrings* [29, 80, 86], i.e. sequences of bits (0/1) which serve as compact combinatorial representations of the denotations of logical formulas. In this paper, we focus on bitstrings of length 4, which allow us to encode 2^4 = 16 formulas from logical systems such as classical propositional logic (CPL) and the modal logic S5, as illustrated in Table 1 — where β is the function mapping a formula φ onto its bitstring representation $\beta(\varphi)$. Bitstrings can be characterized in terms of their *level*, i.e. the number of positions with value 1. Hence, the top half in Table 1 contains the 4 level 1 (L1) bitstrings and the 4 L3 bitstrings; the bottom half in Table 1 consists of the 6 L2 bitstrings as well as the L0 and L4 bitstrings. The standard Boolean operations of meet, join and complement can straightforwardly be defined on this set of 16 bitstrings,[6] yielding the Boolean algebra $\mathbb{B}_4 = \{0,1\}^4$ [46]. The Aristotelian relation holding between formulas φ and ψ can then easily be determined by computing the meet and join of their bitstring counterparts $\beta(\varphi)$ and $\beta(\psi)$. Two bitstrings b_1 and b_2 of length 4 are:

contradictory (CD)	iff	$b_1 \wedge b_2 = 0000$	and	$b_1 \vee b_2 = 1111$,
contrary (C)	iff	$b_1 \wedge b_2 = 0000$	and	$b_1 \vee b_2 \neq 1111$,
subcontrary (SC)	iff	$b_1 \wedge b_2 \neq 0000$	and	$b_1 \vee b_2 = 1111$,
in subalternation (SA)	iff	$b_1 \wedge b_2 = b_1$	and	$b_1 \vee b_2 \neq b_1$.

Two formulas φ and ψ are *CD* iff they cannot be true together and cannot be false together. Hence, the meet of their bitstrings $\beta(\varphi)$ and $\beta(\psi)$ equals the bottom element 0000 of $\mathbb{B}_4$, whereas their join equals its top element 1111. With C and

[6] These operations are defined bit position by bit position; for example, $\neg 1100 = 0011$, $1100 \wedge 1010 = 1000$ and $1100 \vee 1010 = 1110$.

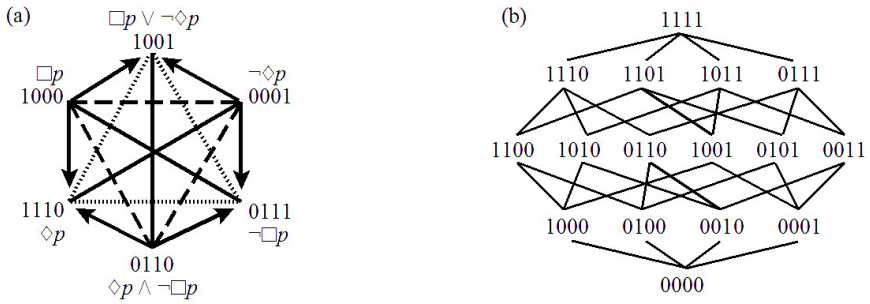

Figure 3: 2D visualizations: (a) JSB hexagon for a fragment of $\mathbb{B}_4$, (b) Hasse diagram for $\mathbb{B}_4$.

SC, one of the two identity conditions of CD is negated: contraries may be false together, while subcontraries may be true together. The set of Aristotelian relations is fundamentally 'hybrid': the *opposition* relations CD, C and SC are defined using the top and bottom elements, while the *implication* relation SA is defined in terms of the related bitstrings b_1 and b_2 themselves [83].

Figure 3 presents two standard 2D visualizations, viz. an Aristotelian hexagon for a fragment of $\mathbb{B}_4$ and a Hasse diagram for $\mathbb{B}_4$ itself. Both diagrams have *central symmetry*: contradictory bitstrings are located at diametrically opposed vertices of the diagram and at the same distance from its centre. Furthermore, in the Hasse diagram, the logical ordering of *levels* corresponds to the vertical geometrical ordering of *lines*, from L0 at the bottom up to L4 at the top.

3 Two Types of 3D Visualizations of $\mathbb{B}_4$

3.1 Cube-based Diagrams

The first type of 3D visualization of $\mathbb{B}_4$ is based on the *rhombic dodecahedron (RDH)* in Figure 4(a), a convex polyhedron with 12 rhombic faces, 14 vertices and 24 edges. This visualization was first proposed by Smessaert [80] and later adopted by Demey [18, 82].[7] The close connection between RDH and both the cube and the octahedron — see Figure 4(b) — is due to RDH being the *dual* of a cuboctahedron (see [84] for more details).

[7]Two closely related cube-based 3D visualizations — viz. Sauriol's tetra(kis-)hexahedron [78] and Moretti and Pellissier's tetraicosahedron [60, 68] — are briefly compared to RDH in [82, 84]. Furthermore, [28] provides a detailed comparative analysis of the correspondence between logical and geometrical distance (cf. Subsection 6.2 of the present paper) in the three cube-based visualizations as well as the tetrahedron-based visualization.

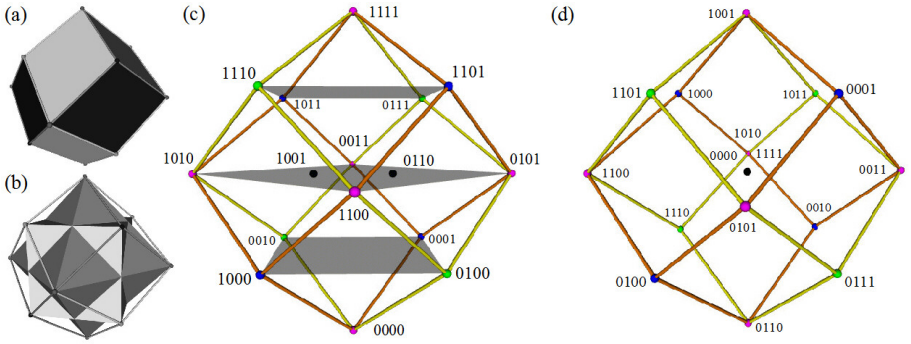

Figure 4: (a) RDH, (b) RDH as a combination of a cube and an octahedron, (c) Hasse RDH, (d) Aristotelian RDH.

The RDH has been used both as a Hasse diagram [54, 96] and as an Aristotelian diagram [80, 84] for $\mathbb{B}_4$; see Figures 4(c) and (d), respectively. As was discussed in [24], both can be seen as vertex-first parallel projections of a 4D hypercube, but along different projection axes. The Hasse RDH results from using the axis defined by the hypercube's vertices for the bitstrings 1001 and 0110, whereas the Aristotelian RDH results from using the axis defined by the vertices for 0000 and 1111. As a consequence, the 2 *non-contingent* bitstrings 0000 and 1111 coincide in the centre of the Aristotelian RDH in Figure 4(d), whereas the 14 *contingent* bitstrings end up at its vertices, as was already observed in [78, 80]. This is the geometric motivation for the diagrammatic convention that Aristotelian diagrams only represent contingent bitstrings.[8] Standard coordinates of the vertices of the Aristotelian RDH are given by the function $c_{RDH} : \mathbb{B}_4 \to \mathbb{R}^3$ in Table 2 (with $\mathbb{R}^3$ being 3D Euclidean space). Finally, note that, just like the 2D Hasse diagram in Figure 3(b), the 3D Hasse RDH in Figure 4(c) has a uniform upward direction of entailment, and is thus *level-preserving*, going from L0 at the bottom up to L4 at the top.[9]

[8]The non-contingent bitstrings enter into many 'vacuous' relations with the contingent ones, e.g. 0000 is contrary to and implies any contingency, while 1111 is subcontrary to and implied by any contingency.

[9]There also exists a strong connection with work in crystallography and digital geometry [50, 66, 87, 88, 93]. In particular, the corresponding Voronoi voxel of the face-centered cubic lattice is exactly the 3D shape of the RDH. This connection will be explored in more detail in future research. Thanks to an anonymous reviewer for pointing us in this direction.

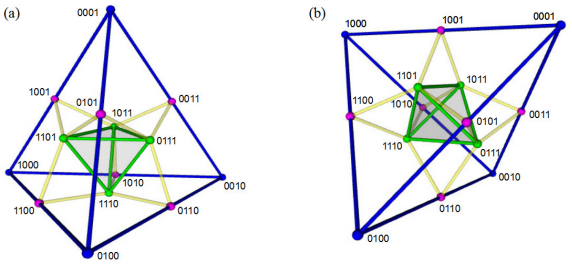

Figure 5: NTH: (a) vertex-face perspective, (b) edge perspective.

3.2 Tetrahedron-based Diagrams

Another 3D visualization of $\mathbb{B}_4$ is the *nested tetrahedron (NTH)* in Figure 5(a). This visualization was first proposed by Ciucci, Dubois and Prade [13, 33], although recent historical research has shown that a predecessor of it was already used by the 19th-century logician (and novelist) Lewis Carroll [8, 61].[10] Because a tetrahedron is *self-dual*, connecting the centres of its 4 faces yields a small, 'nested' tetrahedron. The 14 contingent bitstrings of $\mathbb{B}_4$ are represented by the 8 vertices of the big and small tetrahedra, and the midpoints of the 6 edges of the big tetrahedron.

Note that in the following sections we will not be adopting the classical perspective on the tetrahedron — i.e. of a pyramid standing on its triangular base, as in Figure 5(a) — but rather that of the tetrahedron standing on one edge, as in Figure 5(b). This perspective yields coordinates for NTH's vertices as given by the function $c_{NTH} : \mathbb{B}_4 \to \mathbb{R}^3$ in Table 2, and facilitates the visual comparison with the Aristotelian RDH, since $c_{NTH}(b) = c_{RDH}(b)$ for all L1 bitstrings b.[11]

4 Representing Implication Relations

Having introduced the Boolean algebra $\mathbb{B}_4$ and its cube- and tetrahedron-based 3D visualizations, we now turn toward a detailed comparison of the cognitive effectiveness of these diagrams. In this section, we start by focusing on the representation of the implication relations.

Both in the 2D visualization of a Hasse diagram in Figure 3(b) of Section 2 and in its 3D counterpart of the Hasse RDH in Figure 4(c) of Section 3, two closely re-

[10] Just like RDH, NTH is a vertex-first projection of a 4D hypercube along the axis defined by the vertices for 0000 and 1111 — although NTH results from a *perspective* projection whereas RDH results from a *parallel* projection. Consequently, just like RDH, NTH has the non-contingent bitstrings 0000 and 1111 coinciding in its centre, as observed in [13, 33].

[11] Furthermore, both NTH and RDH are centred around $\mathbf{o} = (0, 0, 0)$, i.e. the origin of $\mathbb{R}^3$, and $c_{RDH}(0000) = c_{NTH}(0000) = c_{RDH}(1111) = c_{NTH}(1111) = \mathbf{o}$.

Table 2: The coordinate functions $c_{RDH} : \mathbb{B}_4 \to \mathbb{R}^3$ and $c_{NTH} : \mathbb{B}_4 \to \mathbb{R}^3$.

$c_{NTH}(b)$	$c_{RDH}(b)$	b	$\neg b$	$c_{RDH}(\neg b)$	$c_{NTH}(\neg b)$
$(-1,1,-1)$	$(-1,1,-1)$	1000	0111	$(1,-1,1)$	$(1/3,-1/3,1/3)$
$(-1,-1,1)$	$(-1,-1,1)$	0100	1011	$(1,1,-1)$	$(1/3,1/3,-1/3)$
$(1,-1,-1)$	$(1,-1,-1)$	0010	1101	$(-1,1,1)$	$(-1/3,1/3,1/3)$
$(1,1,1)$	$(1,1,1)$	0001	1110	$(-1,-1,-1)$	$(-1/3,-1/3,-1/3)$
$(-1,0,0)$	$(-2,0,0)$	1100	0011	$(2,0,0)$	$(1,0,0)$
$(0,0,-1)$	$(0,0,-2)$	1010	0101	$(0,0,2)$	$(0,0,1)$
$(0,1,0)$	$(0,2,0)$	1001	0110	$(0,-2,0)$	$(0,-1,0)$

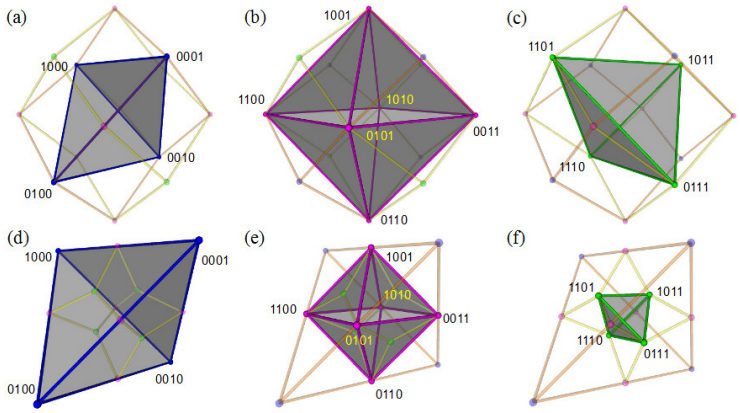

Figure 6: RDH: (a) L1, (b) L2, (c) L3; NTH: (d) L1, (e) L2, (f) L3.

lated types of uniformity can be observed, namely the general upward direction of the implication relations and the systematic visualization of the levels of the Boolean algebra: in a Hasse diagram the levels are visualized as (horizontal) hyperplanes that are orthogonal to the general (vertical) implication direction. This type of uniformity is a clear instance of the *congruence principle*, according to which the structure and content of the visualization should correspond to the represented logical structure and content [90, 91].

Let us now consider to what extent this cognitive principle applies to the relation between the logical levels in $\mathbb{B}_4$ on the one hand, and the geometrical structures of RDH and NTH on the other. Ignoring the two non-contingent elements, $\mathbb{B}_4$ consists of 4 L1 elements, 6 L2 elements and 4 L3 elements (see Section 2). Figure 6 shows the L1/L2/L3 distribution in RDH and NTH.

First of all, a fundamental geometrical similarity can be observed between RDH and NTH as far as the representation of the 6 L2 elements is concerned:

both in Figure 6(b) and in Figure 6(e) the L2 elements correspond to the 6 vertices of an octahedron. As for the L1 and L3 elements, by contrast, the situation is somewhat more complex. On the one hand, the 4 L1 elements constitute a tetrahedron both in Figure 6(a) and Figure 6(d), and the same holds for the 4 L3 elements, as is clear from the two tetrahedra in Figures 6(c) and 6(f). On the other hand, however, there is a fundamental difference between RDH and NTH concerning the relationship between the two tetrahedra. Within RDH, the L1 tetrahedron in Figure 6(a) and the L3 tetrahedron in Figure 6(c) have the *same size* and 'interlock' with each other to yield the 8 vertices of the cube inside RDH — see Figure 4(b). Within NTH, by contrast, the 4 L1 elements constitute the *big* tetrahedron in Figure 6(d), whereas the 4 L3 elements constitute the *small* tetrahedron in Figure 6(f). Despite this considerable difference in size, however, the two NTH tetrahedra are no less 'interlocking' than their RDH counterparts: the small L3 tetrahedron is the dual of the big L1 tetrahedron, thus illustrating the self-dual nature of the tetrahedron (see Section 3).

It is clear that the original visual uniformity of the 2D and 3D Hasse diagrams — levels being visualized as (horizontal) hyperplanes orthogonal to the general (vertical) implication direction — is lost, both in RDH in Figures 6(a-c) and in NTH in Figures 6(d-f): there is no way in which the implications can be said to be 'going upward along a single dimension', first from the L1 plane to the L2 plane and then from the L2 plane to the L3 plane. Still, we argue that NTH observes the congruence principle much better than RDH, albeit in a different way: logical levels no longer correspond to parallel hyperplanes ordered along one vertical dimension, but rather to the geometrical dimensions themselves. The natural geometrical ordering of zero-dimensionality for vertices, one-dimensionality for edges and two-dimensionality for faces thus corresponds to the logical ordering of the levels L1, L2 and L3. The 4 L1 *vertices* of the big tetrahedron in Figure 6(d) are straightforwardly of dimension *zero*. For the L2 and L3 elements, however, a reconceptualization is required. The 6 L2 elements in Figure 6(e) can not only be thought of as the 6 vertices of an octahedron, but also as the midpoints of the 6 *edges* of the big L1 tetrahedron, thus making them elements of dimension *one*. Analogously, the 4 L3 elements in Figure 6(f) can not only be seen as the 4 vertices of the small tetrahedron, but also as the midpoints of the 4 *faces* of the big L1 tetrahedron, thus making them elements of dimension *two*.

The isomorphism between the logical structure of $\mathbb{B}_4$ and the geometrical structure of NTH can thus be extended to the logical operation of 'taking the join' and the geometrical operation of 'taking the midpoint'. The join of any two L1 elements — e.g. 1000 and 0001 — is the L2 element located in the middle of the edge connecting the vertices of those two L1 elements — in our example: 1001. Similarly, the join of any three L1 elements — e.g. 1000, 0100 and 0001 — is the L3

element occurring in the middle of the face defined by the vertices of those three L1 elements — in our example: 1101. Furthermore, the join of a contrary pair of L1 and L2 elements — e.g. 1000 and 0110 — is the L3 element located in the middle of the face defined by the vertex and the opposing edge corresponding to those L1 and L2 elements, respectively — in our example: 1110. Finally, the join of any two non-CD L2 elements is again the L3 element occurring in the middle of the face defined by the two edges corresponding to those two L2 elements — e.g. 1001 and 1100 at the midpoints of the top and left edges in Figure 6(e) have as their join 1101, which is in the middle of the front left face in Figure 6(f).

Summing up, just like the 2D and 3D Hasse diagrams discussed earlier, NTH directly visualizes the logical levels, although the visualization strategy behind the isomorphism is fundamentally different. RDH, by contrast, is not level-preserving at all: logical levels do not correspond to parallel hyperplanes ordered along one vertical dimension, and not to zero-, one- and two-dimensionality either. This distortion of congruence is due to the 4 L1 and the 4 L3 elements being intertwined as 8 geometrically equivalent vertices of a cube. In other words, RDH no longer allows us to draw a distinction which is crucial from the point of view of the implication relation in $\mathbb{B}_4$, and hence the isomorphism between the logical and geometrical structures breaks down.

5 Representing Opposition Relations

5.1 (Sub)contrariety and Interlocking Tetrahedra

We now turn to the opposition relations as introduced in Section 2. It has become clear from the previous subsection that the logical notion of level plays a crucial role in the analysis of the implication relation of *subalternation*: this relation systematically holds between elements of lower and higher levels. Furthermore, the notion of level is also important for characterizing the opposition relations: *contrariety* holds between any pair of L1 elements in the tetrahedra of RDH and NTH in Figures 6(a) and 6(d), and similarly *subcontrariety* holds between any pair of L3 elements in the tetrahedra in Figures 6(c) and 6(f).[12] Finally, the absence of any Aristotelian (opposition or implication) relation — i.e. logical independence or *unconnectedness* [83] — precisely occurs between the 12 pairs of L2 elements which correspond to the 12 edges of the octahedra in Figure 6(b) for RDH and Figure 6(e) for NTH.[13]

[12] Moretti [60, Chapter 11] uses the term 'bi-simplex' to generalize such correlated constellations of contrariety and subcontrariety.

[13] The facts that (i) the L1 elements constitute a contrariety tetrahedron, (ii) the L3 elements constitute a subcontrariety tetrahedron, and (iii) the L2 elements constitute an unconnectedness octahedron

As demonstrated above, however, RDH and NTH differ from one another as to whether or not the L1 and L3 elements are visualized equivalently: in RDH the L1 and L3 tetrahedra have the same size and are intertwined in a cube, whereas in NTH the small L3 tetrahedron is nested inside the big L1 tetrahedron. Hence the fundamental question of congruence arises: do the geometrical differences between the opposition relations of contrariety and subcontrariety in NTH reflect any fundamental logical differences in $\mathbb{B}_4$? At least two answers seem possible. Firstly, one could argue that contrariety is a stronger opposition relation than subcontrariety, since the former involves incompatibility whereas the latter does not.[14] The greater geometrical distance between the vertices of the big tetrahedron in Figure 6(d) would then be isomorphic to the greater logical distance between L1 contraries [90, 91]. On this view, NTH would reveal a greater degree of congruence between logical and geometrical distance than RDH. Secondly, one could argue in favour of treating contrariety and subcontrariety on a par: starting from the definition of contradiction which involves two identity conditions (cf. Section 2), both contrariety and subcontrariety negate one condition and maintain the other one, but in different conjuncts of the definition. Since they deviate from contradiction in 'opposite' directions, they are each other's 'mirror image'. On this more symmetric view, contrariety and subcontrariety have an equal logical status, and hence RDH would exhibit a greater degree of congruence between logical and geometrical structure than NTH.

5.2 Contradiction and Central Symmetry

The visual representation of *contradiction* in RDH and NTH is given in Figure 7(a-b) and (c-d), respectively. As was the case with (sub)contrariety in the previous subsection, the visualization of contradiction simultaneously reveals similarities as well as fundamental differences between RDH and NTH. Starting with the similarities, we can observe that both RDH and NTH make a clear geometrical distinction between two subtypes of contradiction. On the one hand, there are 4 pairs of contradictories (PCDs) consisting of an L1 and an L3 element: in Figure 7(a) these correspond to the 4 diagonals of the cube inside RDH, whereas in Figure 7(c) each L1 vertex of the big tetrahedron is connected to its 'opposite' L3 vertex of the small tetrahedron. On the other hand, there are 3 PCDs consisting of two L2 elements: both in Figure 7(b) and (d) these correspond to the 3 diagonals of the octahedra inside RDH and NTH, respectively. As for RDH, this geometric distinction between two types of PCDs plays a crucial role in establishing an exhaustive anal-

in RDH as well as NTH are also noted in [61].

[14] For example, Aristotle himself did not recognize subcontrariety as a genuine relation of opposition, claiming that subcontraries are "only verbally opposed" [51, p. 11].

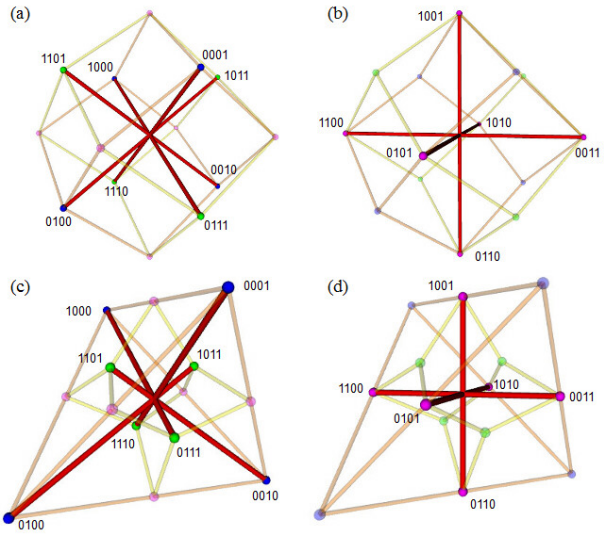

Figure 7: Contradiction in RDH: (a) L1-L3, (b) L2-L2; in NTH: (c) L1-L3, (d) L2-L2.

ysis of its Aristotelian subdiagrams [82]. We return to this topic of subdiagrams in Section 7, especially for the comparison between RDH and NTH, but overall, this subdivision into four L1-L3 PCDs and three L2-L2 PCDs counts as a strong case of logico-geometrical congruence, both for RDH and for NTH.

In spite of this initial similarity between the two visualizations, they also exhibit a number of fundamental differences in representing the contradiction relation. A first major difference concerns the property of *central symmetry*. As mentioned in Section 2, contradictory bitstrings in 2D Aristotelian diagrams, such as the square or the hexagon, are standardly located at diametrically opposed vertices of the diagram and at the same distance from its centre. Moving to the 3D visualizations, central symmetry turns out to hold for the L2-L2 PCDs in both RDH and NTH: the vertices on the 3 'octahedral' diagonals in Figures 7(b) and 7(d) are located at the same distance of the diagrams' centres. The same holds for the L1-L3 PCDs on the 4 'cubic' diagonals of RDH in Figure 7(a). In NTH, by contrast, the 4 contradictory L1-L3 diagonals in Figure 7(c) are no longer symmetrical: the 4 L3 vertices are located at a much shorter distance from the centre than their contradictory L1 counterparts.[15]

[15]For example, concerning the PCD 1000-0111, we have that $d_E(c_{NTH}(1000), \mathbf{o}) = 1.73 \neq 0.58 = d_E(c_{NTH}(0111), \mathbf{o})$, where d_E is the Euclidean distance measure on $\mathbb{R}^3$ and c_{NTH} is the NTH coordinate function defined in Table 2.

Logically speaking, contradiction is not just symmetric — a property which it shares with (sub)contrariety — but also the only *functional* opposition relation: every bitstring is contradictory to exactly one bitstring, whereas it may be (sub)contrary to many different bitstrings. Furthermore, this symmetry holds in exactly the same way for the L1-L3 PCDs as for the L2-L2 PCDs. These logical properties of symmetry and functionality are nicely captured geometrically by the property of central symmetry: every vertex stands in central symmetry to exactly one vertex. RDH has central symmetry for both the L1-L3 PCDs and the L2-L2 PCDs, whereas NTH only has central symmetry for the latter. Hence, NTH exhibits a lower degree of overall logico-geometrical congruence than RDH.[16]

6 Combining Implication and Opposition

6.1 Subalternation, Contrariety and Collinearity

In Sections 4 and 5 we have explored how RDH and NTH visualize the implication and opposition relations, respectively. We now turn to the interplay of these two types of relations in RDH as well as NTH. A major issue with NTH in this regard is that it contains several triples of collinear vertices, viz. those corresponding to two contrary elements and their join.

A first type of collinearity can be found on the edges of NTH, and involves pairs of contrary L1 elements and their L2 joins. Consider, for example, the vertices corresponding to the elements 1000, 0001 and 1001 in Figure 8(a). As to the Aristotelian relations holding between these bitstrings, we not only have a contrariety between 1000 and 0001, but also subalternations from both 1000 and 0001 to 1001. However, because the vertices corresponding to these three bitstrings are collinear, the visualization of the contrariety between 1000 and 0001 (viz. the top edge of NTH) overlaps/coincides with the visualizations of the subalternations from 1000 to 1001 and from 0001 to 1001 (viz. the two 'halves' of the top edge of NTH).

A second type of collinearity can be found on the medians of the faces of NTH, and involves pairs of contrary L1 and L2 elements and their L3 joins. Consider, for example, the vertices corresponding to the elements 1000, 0110 and 1110 in Figure 8(b). As to the Aristotelian relations holding between these bitstrings, we again have a contrariety (between 1000 and 0110) that overlaps/coincides with the two subalternations from 1000 and 0110 to 1110.

In both types of collinearity, the overlap between the three Aristotelian rela-

[16] The differences between RDH and NTH with respect to central symmetry are also noted in [61], but without explicitly appealing to the congruence principle from diagram design.

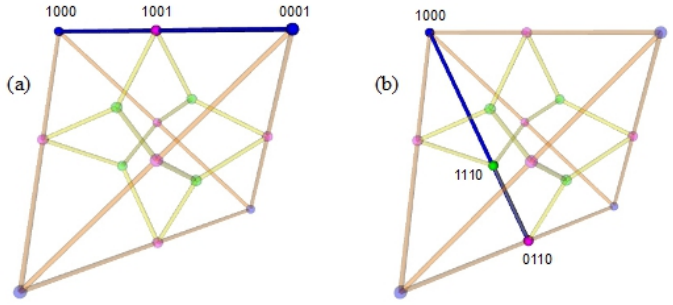

Figure 8: Collinearities in NTH corresponding to two subalternations and one (a) L1-L1 contrariety (b) L1-L2 contrariety

tions involved might cause the user looking at NTH to experience difficulties in properly distinguishing between these relations. This can be considered a violation of Tversky's *apprehension principle*, according to which "the structure and content of the visualization should be readily and accurately perceived and comprehended" [90, p. 37].[17] This preference for non-overlapping visualizations also shows up in the design of other types of logical diagrams, such as Euler diagrams (consider, for example, the second wellformedness condition in [41], which requires that contours of Euler diagrams not be concurrent).

It should be noted that the various[18] collinearities in NTH (and hence, the overlappings between opposition and implication relations) are a direct consequence of the design strategy to visualize the logical operation of 'taking the join' (of contrary elements) by means of the geometrical operation of 'taking the midpoint' (in order to create a strong isomorphism between the geometrical ordering of 0-, 1- and 2-dimensional shapes and the logical ordering of L1, L2 and L3 bitstrings; cf. Section 4). After all, given any two vertices, the midpoint of the line segment defined by those two vertices will automatically be collinear with those two vertices. Hence, even though this design strategy works very well *locally*, i.e. if only the implication relations are taken into account, it fares much worse *globally*, i.e. if both opposition and implication relations are taken into account. Furthermore, since there are 18 collinearities in total (cf. Footnote 18), each of which involves 1 contrariety overlapping with 2 subalternations, and $\mathbb{B}_4$ contains 18 contrarieties and 36 subalternations [18, p. 334], it follows that *every* contrariety in $\mathbb{B}_4$ ends

[17] Both types of collinearity in NTH are also hinted at in [13, 33], but without explicitly appealing to diagram design principles.

[18] More precisely, since there are 4 L1 vertices, NTH contains $\binom{4}{2} = 6$ collinearities of the first type. Furthermore, since there are 4 L3 faces, each of which has 3 medians, NTH contains $4 \times 3 = 12$ collinearities of the second type.

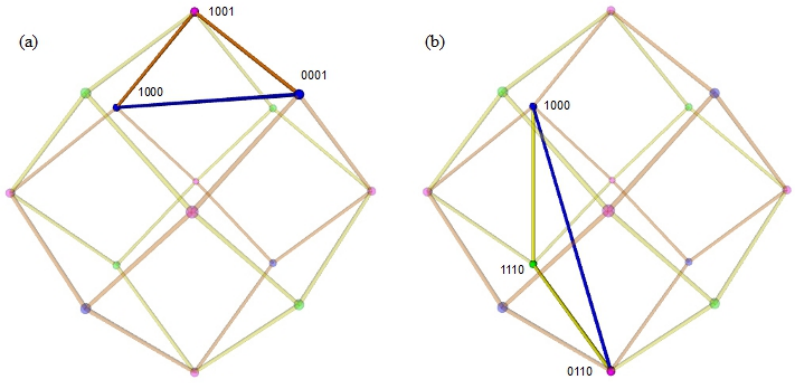

Figure 9: Triangles in RDH corresponding to two subalternations and one (a) L1-L1 contrariety (b) L1-L2 contrariety.

up overlapping with other Aristotelian relations. This shows that the NTH visualization of the interplay between implication and opposition relations is highly problematic.

In sharp contrast to NTH, the RDH visualization of $\mathbb{B}_4$ does not have any triples of collinear vertices. Consequently, all Aristotelian relations holding between the elements of $\mathbb{B}_4$ (oppositions and implications alike) are visualized by means of distinct (non-coinciding) lines (either edges of RDH itself or lines crossing the interior of RDH). In particular, pairs of two L1 vertices and their L2 joins are visualized in RDH by means of triangles, and the same holds for pairs of L1 and L2 vertices and their L3 joins. For example, the vertices corresponding to the elements 1000, 1001 and 0001 are collinear in NTH, but constitute a triangle in RDH; compare Figures 8(a) and 9(a). Similarly, the vertices corresponding to the elements 1000, 0110 and 1110 are collinear in NTH, but constitute a triangle in RDH; compare Figures 8(b) and 9(b). The systematic avoidance of unwanted overlappings between visual elements means that RDH is much more in accordance with the apprehension principle.

6.2 Logical and Geometrical Distance

Since the elements of the Boolean algebra $\mathbb{B}_4$ are represented by means of bitstrings (of length 4), we can measure the 'logical distance' between them by counting the number of bits that need to be flipped to go from one element to the other. Formally, this corresponds to the notion of *Hamming distance* (d_H) from coding theory [77]. For all bitstrings $b, b' \in \mathbb{B}_4$ it trivially holds that $0 \leq d_H(b, b') \leq 4$, and $d_H(b, b') = 0$ iff $b = b'$. Table 3 lists all nonzero Hamming distances

Table 3: Logical distance (d_H) and geometrical distance in RDH (d_{RDH}) and NTH (d_{NTH}).

$d_H(b,b')$	$L(b)$	$L(b')$	$R(b,b')$	example	$d_{RDH}(b,b')$	$d_{NTH}(b,b')$
1	1	2	SA	1000-1100	1.73	1.41
1	2	3	SA	1100-1110	1.73	0.82
2	1	3	SA	1000-1110	2	1.63
2	1	1	C	1000-0001	2.83	2.83
2	3	3	SC	1110-0111	2.83	0.94
2	2	2	—	1100-0110	2.83	1.41
3	1	2	C	1000-0110	3.32	2.45
3	2	3	SC	1100-0111	3.32	1.41
4	1	3	CD	1000-0111	3.46	2.31
4	2	2	CD	1100-0011	4	2

$d_H(b,b')$, along with the levels $L(b)$ and $L(b')$ of the bitstrings b and b', the Aristotelian relation R holding between b and b', a concrete pair of bitstrings illustrating this relation, and the geometrical distances between b and b' in the two 3D visualizations — in particular, $d_{RDH}(b,b') := d_E(c_{RDH}(b), c_{RDH}(b'))$ and $d_{NTH}(b,b') := d_E(c_{NTH}(b), c_{NTH}(b'))$, where d_E is the usual Euclidean distance measure on $\mathbb{R}^3$ and c_{RDH} and c_{NTH} are the coordinate functions introduced in Table 2.[19]

It should be emphasized that the notion of Hamming distance cuts across the implication and opposition relations; for example, Table 3 shows that Hamming distance 2 occurs in the case of a subalternation from an L1 to an L3 bitstring, but also in the case of two contrary L1 bitstrings, in the case of two subcontrary L3 bitstrings, and even in the case of two unconnected L2 bitstrings (which do not stand in any Aristotelian relation whatsoever). Furthermore, it also bears emphasizing that one should not focus on the precise numerical values shown in Table 3, since these values are based on the particular coordinate functions c_{RDH} and c_{NTH} (cf. Table 2), which yield polyhedra of different measures (i.e. different volumes). Rather, one should focus on the ordering and the ratios of these numerical values, which is exactly what we will do now.

As can be seen in Table 3, increasing Hamming distances systematically corre-

[19]Note that the logical distance d_H can alternatively also be thought of as the Manhattan distance on $\{0,1\}^4 \subseteq \mathbb{R}^4$, i.e. $d_H(b,b') = \sum_{i=1}^4 |b_i - b'_i|$. From this perspective, logical distance (d_H) and geometrical distance (d_E) both turn out to be special cases of Minkowski distance ($\sum_{i=1}^4 |b_i - b'_i|^p)^{1/p}$, by taking $p = 1$ and $p = 2$, respectively [32].

spond to increasing geometrical distances in RDH. More formally, for all bitstrings $b_1, b_2, b_3, b_4 \in \mathbb{B}_4$ we have

$$d_H(b_1, b_2) < d_H(b_3, b_4) \implies d_{RDH}(b_1, b_2) < d_{RDH}(b_3, b_4). \tag{1}$$

Note that the corresponding $\Longleftarrow$-claim does *not* hold,[20] but a slightly modified version of it does hold: for all bitstrings $b_1, b_2, b_3, b_4 \in \mathbb{B}_4$ we have

$$d_H(b_1, b_2) \leq d_H(b_3, b_4) \Longleftarrow d_{RDH}(b_1, b_2) < d_{RDH}(b_3, b_4). \tag{2}$$

These principles show that the RDH visualization of $\mathbb{B}_4$ exhibits a fundamental congruence between logical distance (d_H) and geometrical distance (d_{RDH}).

In the NTH visualization, by contrast, this logico-geometrical congruence is lost: Table 3 shows that the condition $d_{NTH}(b_1, b_2) < d_{NTH}(b_3, b_4)$ is compatible with $d_H(b_1, b_2) \leq d_H(b_3, b_4)$,[21] but also with $d_H(b_1, b_2) > d_H(b_3, b_4)$.[22]

A special case of this (in)congruence in RDH and NTH, which was first studied in [85], is concerned with *maximal* logical and geometrical distance. Logically speaking, one can argue that contradiction is the 'strongest' Aristotelian relation, since it is the only relation that involves not one, but two identity conditions (cf. the discussion in Section 2) [23, 69]. Consequently, every bitstring $b \in \mathbb{B}_4$ has exactly one contradictory, $\neg b$, whereas it has multiple contraries and/or subcontraries [83, 86]. In terms of Hamming distances, turning a bitstring b into its contradictory, $\neg b$, involves switching the values in *all* of its bit positions. It thus follows that for all bitstrings $b \in \mathbb{B}_4$ we have

$$\neg b = \arg\max_{x \in \mathbb{B}_4} d_H(b, x). \tag{3}$$

As can be seen in Table 3, the maximal Hamming distance (viz. 4) indeed occurs with the contradictions. Additionally, we observe that in the RDH visualization of $\mathbb{B}_4$, the following holds for all bitstrings $b \in \mathbb{B}_4$:[23]

$$\neg b = \arg\max_{x \in \mathbb{B}_4} d_{RDH}(b, x). \tag{4}$$

[20] For example, we have $d_{RDH}(1000, 1110) = 2 < 2.83 = d_{RDH}(1000, 0001)$, and yet $d_H(1000, 1110) = 2 = d_H(1000, 0001)$.

[21] For example, we have $d_{NTH}(1000, 1100) = 1.41 < 2.45 = d_{NTH}(1000, 0110)$ and also $d_H(1000, 1100) = 1 < 3 = d_H(1000, 0110)$.

[22] For example, we have $d_{NTH}(1100, 0111) = 1.41 < 2.83 = d_{NTH}(1000, 0001)$, and yet $d_H(1100, 0111) = 3 > 2 = d_H(1000, 0001)$.

[23] Note that the geometrical distance in RDH is different for the L1-L3 and L2-L2 contradictions, viz. 3.46 and 4, respectively. Nevertheless, both types of contradictions give rise to one and the same Hamming distance, viz. 4 (recall that the $\Longleftarrow$-version of (1) does *not* hold, but that (2) does hold).

Putting (3) and (4) together, we obtain the following restricted version of the logico-geometrical congruence principle for distances, which states that in the RDH visualization of $\mathbb{B}_4$, 'maximal logical distance' directly corresponds to 'maximal geometrical distance': for all $b \in \mathbb{B}_4$ it holds that

$$\arg\max_{x \in \mathbb{B}_4} d_H(b, x) = \arg\max_{x \in \mathbb{B}_4} d_{RDH}(b, x). \tag{5}$$

Moving from RDH to NTH, it turns out that even this restricted version of the logico-geometrical congruence principle does not hold in general. On the one hand, we can see in Table 3 that for any L3 bitstring b, it does hold that

$$\arg\max_{x \in \mathbb{B}_4} d_H(b, x) = \neg b = \arg\max_{x \in \mathbb{B}_4} d_{NTH}(b, x). \tag{6}$$

On the other hand, Table 3 also shows that for all L1 and L2 bitstrings b, there exists a bitstring b' that is *not* contradictory to b (i.e. $b' \neq \neg b$), and yet $d_{NTH}(b, b') > d_{NTH}(b, \neg b)$,[24] which means exactly that

$$\arg\max_{x \in \mathbb{B}_4} d_H(b, x) = \neg b \neq \arg\max_{x \in \mathbb{B}_4} d_{NTH}(b, x). \tag{7}$$

The fact that the restricted logico-geometrical congruence principle for distances succeeds for L3 but fails for L1 is clearly related to the fact that logical negation does not correspond to central symmetry in the NTH. After all, logical negation establishes a systematic connection between both logical levels: b is an L1 bitstring iff $\neg b$ is an L3 bitstring. To understand this better, note that in polyhedral Aristotelian diagrams in which negation does correspond to central symmetry (such as the RDH), the restricted logico-geometrical congruence principle holds for L1 bitstrings iff it holds for L3 bitstrings.

Everything we have said so far about logical and geometrical distances involves *ordinal* comparisons ($<$, $\geq$, $\max$, etc.). However, one can also take a more fine-grained approach to these distances, and focus on their *ratios*. As was first noted in [13, 33], the NTH visualization fares much better from this ratio perspective. Consider, for example, the case of two contrary L1 bitstrings and their L2 join, such as 1000, 0001 and 1001; cf. Figures 8(a) and 9(a). These bitstrings give rise to the following ratio of Hamming distances:

$$\langle d_H(1000, 0001) \,:\, d_H(1000, 1001) \,:\, d_H(0001, 1001) \rangle = \langle 2 : 1 : 1 \rangle \tag{8}$$

[24] For example, the contradictory of the L1 bitstring 1000 is 0111, and yet we have $d_{NTH}(1000, 0001) = 2.83 > 2.31 = d_{NTH}(1000, 0111)$. Similarly, the contradictory of the L2 bitstring 1100 is 0011, and yet we have $d_{NTH}(1100, 0010) = 2.45 > 2 = d_{NTH}(1100, 0011)$.

As can be seen in Table 3, the RDH and NTH visualizations give rise to the following ratios of geometrical distances:

$$\langle d_{RDH}(1000, 0001) \,:\, d_{RDH}(1000, 1001) \,:\, d_{RDH}(0001, 1001)\rangle = \langle 2\sqrt{2} : \sqrt{3} : \sqrt{3}\rangle \quad (9)$$

$$\langle d_{NTH}(1000, 0001) \,:\, d_{NTH}(1000, 1001) \,:\, d_{NTH}(0001, 1001)\rangle = \langle 2\sqrt{2} : \sqrt{2} : \sqrt{2}\rangle \quad (10)$$

Comparing (8–10), we see that in RDH, the geometrical distances do not have the same ratio as their corresponding logical distances; in NTH, by contrast, the logical and geometrical distances do have the same ratios.

A second example concerns the case of contrary L1 and L2 bitstrings, and their L3 join, such as 1000, 0110 and 1110; cf. Figures 8(b) and 9(b). These bitstrings give rise to the following ratio of Hamming distances:

$$\langle d_H(1000, 0110) \,:\, d_H(1000, 1110) \,:\, d_H(0110, 1110)\rangle = \langle 3 : 2 : 1\rangle \quad (11)$$

And we have the following ratios of geometrical distances:

$$\langle d_{RDH}(1000, 0110) : d_{RDH}(1000, 1110) : d_{RDH}(0110, 1110)\rangle = \langle \sqrt{11} : 2 : \sqrt{3}\rangle \quad (12)$$

$$\langle d_{NTH}(1000, 0110) : d_{NTH}(1000, 1110) : d_{NTH}(0110, 1110)\rangle = \langle \sqrt{6} : \frac{2}{3}\sqrt{6} : \frac{1}{3}\sqrt{6}\rangle \quad (13)$$

Once again, we observe that in RDH, the logical and geometrical distances do not have the same ratios, whereas in NTH, they do. Examples such as these show that if we focus on ratios of distances rather than on their relative ordering, then NTH turns out to embody a much stronger logico-geometrical congruence than RDH.

7 Subdiagram Embeddings

7.1 Embedding Squares

The description of the internal structure of RDH in [82] crucially relies on the notions of *subdiagram* and *diagram embedding*.[25] The smallest non-trivial such subdiagrams are the Aristotelian squares,[26] which (in the context of $\mathbb{B}_4$) come in three subtypes: the *balanced square* consists of two L1-L3 PCDs, the *unbalanced square* combines one L1-L3 PCD and one L2-L2 PCD, and finally an *unconnected square* consists of two L2-L2 PCDs.[27] The visual representations of the embedding

[25] These notions have also been studied for other types of diagrams, such as Euler diagrams [40], Venn diagrams [43], spider diagrams [92] and algebra diagrams [10].

[26] In this section, the terms 'square' and 'hexagon' are used to refer to any Aristotelian diagram with 2 resp. 3 PCDs, regardless of its concrete geometric properties.

[27] From a purely Aristotelian perspective, the balanced and unbalanced squares are both 'classical', in the sense that they have a contrariety, a subcontrariety, two subalternations and two contradictions; by contrast, the unconnected squares are 'degenerate', in the sense that they only have two contradictions [82, 83].

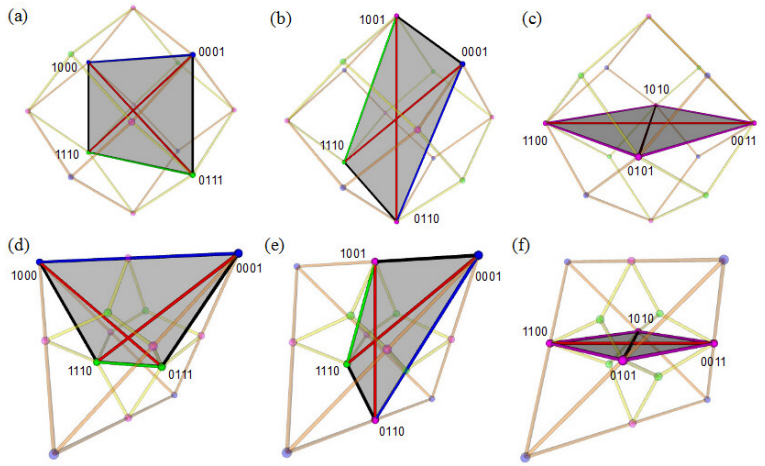

Figure 10: Aristotelian squares in RDH: (a) balanced, (b) unbalanced, (c) unconnected; and in NTH: (d) balanced, (e) unbalanced, (f) unconnected.

of these three subtypes in RDH and NTH are presented in Figures 10(a-c) and 10(d-f), respectively.

Observe, first of all, that the unconnected squares in Figures 10(c) and 10(f) constitute the only subtype that gets a similar representation in RDH and NTH, and that is furthermore actually embedded in the shape of a square. Secondly, as for the balanced squares, the embedding into RDH in Figure 10(a) takes the shape of a proper (i.e. non-square) rectangle — with angles of 90°, equal length and parallel edges for contrariety and subcontrariety as well as for the two subalternations — whereas that into NTH in Figure 10(d) takes the shape of an isosceles trapezium — with different lengths but parallel edges for contrariety and subcontrariety, but same length and non-parallel edges for subalternation. This is another manifestation of the congruence question — namely whether or not the geometrical differences between the opposition relations of contrariety and subcontrariety in NTH reflect fundamental differences in the logical structure of $\mathbb{B}_4$ — which was argued in Section 4 to be answerable either way.

The final subtype of Aristotelian squares to be embedded into RDH and NTH is that of the unbalanced squares in Figures 10(b) and 10(e), respectively. In RDH this yields a parallelogram shape: the angles are no longer 90°, but we still get equal length and parallel edges for contrariety and subcontrariety as well as for the two subalternations. The resulting shape in NTH, by contrast, is a proper quadrilateral, with four different lengths for the (sub)contrariety and the subalternations

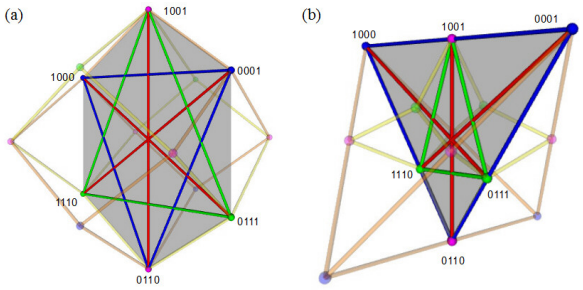

Figure 11: Strong Jacoby-Sesmat-Blanché hexagon in (a) RDH, (b) NTH.

and no parallel edges whatsoever.[28] The logical difference between the balanced and the unbalanced squares is thus visualized either as the minor geometrical difference between rectangle and parallelogram in RDH — cf. Figures 10(a-b) —, or as the more substantial geometrical difference between isosceles trapezium and quadrilateral in NTH — cf. Figures 10(d-e). In terms of congruence, the visual quality of RDH and NTH thus depends on how significant the logical difference between balanced and unbalanced squares is taken to be.

Summing up, the balanced, unbalanced and degenerate squares are embedded inside RDH with the geometrical shapes of squares, proper rectangles and parallelograms, respectively, whereas they are embedded inside NTH as squares, isosceles trapezia and proper quadrilaterals, respectively. The subdiagrams of RDH thus systematically stay closer to the 'ideal' geometrical shape of a (highly regular and symmetric) square than those of NTH, and consequently, they are easier to distinguish visually inside the 3D polyhedron in which they are embedded. From the perspective of the apprehension principle, RDH thus fares much better than NTH.

7.2 Embedding Hexagons

Various families of Aristotelian hexagons exist in $\mathbb{B}_4$, and can thus be embedded inside RDH/NTH [82]. However, we will focus here on the family that is most well-known in artificial intelligence research [11, 12, 16, 94, 95], viz. the so-called strong Jacoby-Sesmat-Blanché (JSB) family, of which some 2D examples were shown in Figures 2(a) and 3(a). When embedded inside RDH, a strong JSB hexagon actually has the geometric shape of a regular hexagon — see Figure 11(a) — and 'slices' RDH into two equal parts [80, 84]. Embedding a strong JSB

[28] Based on the appearance of Figure 10(e), it might look like the NTH vertices for the bitstrings 0001, 1110, 1001 and 0110 are not even coplanar, and thus a fortiori do not form a quadrilateral. However, by considering their coordinates (cf. Table 2), one can see that these four vertices are effectively in a single plane, viz. $x - z = 0$.

hexagon into NTH, by contrast, results in the radically different, 'nested triangular' shape in Figure 11(b) (with a big contrariety triangle on the outside and a small subcontrariety triangle on the inside), which also 'slices' NTH into two equal parts. As far as apprehension of the subdiagrams' shape is concerned, RDH thus fares better than NTH with respect to visualizing its strong JSB hexagon subdiagrams.

Furthermore, two earlier issues with NTH show up again even more strongly here. Firstly, there is the congruence question from Section 5, i.e. to what extent do the geometrical differences between contrariety and subcontrariety reflect differences in the logical structure of $\mathbb{B}_4$? Secondly, the apprehension problem of overlapping contrariety and subalternation relations from Section 6 is multiplied: not only does an L2 element collinearily intervene between two L1 elements at the top edge of the contrariety triangle in Figure 11(b), but so does an L3 element between an L1 and an L2 element at its left and right edges.

Logically speaking, the L1-L1 contrariety is *stronger* than the two L1-L2 contrarieties (there is a bigger 'logical gap' in the former than in the latter two). To ensure congruence between logical and geometrical distance, these different contrarieties are best visualized using lines of different length [49, 90]. And indeed, both contrariety triangles in Figure 11 are isosceles instead of equilateral. However, in RDH the L1-L1 contrariety edge is *shorter* than the two L1-L2 edges, whereas in NTH it is *longer*, which renders NTH more congruent than RDH.[29,30]

8 Conclusion

In this paper we have carried out a detailed comparative analysis of the geometric and cognitive properties of two 3D Aristotelian diagrams for the Boolean algebra $\mathbb{B}_4$, viz. the rhombic dodecahedron (RDH) and the nested tetrahedron (NTH). Our analysis has focused on geometrical notions such as central symmetry, collinearity and distance, and on general cognitive principles from diagram design and information visualization, such as congruence and apprehension.

As stated in Footnote 5, an initial (non-cognitively oriented) comparison between RDH (and related diagrams) and NTH (and related diagrams) was carried out by Moretti [61]. Based on his analysis, Moretti draws some fairly radical conclusions: when visualizing $\mathbb{B}_4$, NTH (and related diagrams) constitute an "unfortunate geometrical choice" (p. 404), an "unlucky configuration" (p. 405) and is "ge-

[29]For example, we have $d_{RDH}(1000, 0001) = 2.83 < 3.32 = d_{RDH}(1000, 0110) = d_{RDH}(0001, 0110)$, whereas $d_{NTH}(1000, 0001) = 2.83 > 2.45 = d_{NTH}(1000, 0110) = d_{NTH}(0001, 0110)$.

[30]The issue of squares and (JSB) hexagons embedded inside RDH vs. NTH is also briefly touched upon in [61].

ometrically suboptimal" (p. 405), whereas RDH (and related diagrams) are "much more informative" (p. 399), "more powerful" (p. 405) and "a stable, geometrically interesting and promising solution" (pp. 405–406).

By contrast, the outcome of the present comparative analysis is much more nuanced in nature. We obtain a clear and detailed perspective on the various advantages and disadvantages of these two visualizations. On the one hand, RDH better observes the congruence principle in visualizing contradiction by central symmetry and in respecting the relative ordering of logical and geometrical distances; furthermore, it better observes the apprehension principle in avoiding overlap between Aristotelian relations and in the regular geometrical shapes with which it visualizes its square and strong JSB hexagon subdiagrams. On the other hand, NTH better observes congruence in representing the logical levels using dimensionality, in respecting ratios of logical geometrical distances, and also in visualizing stronger contrarieties by longer edges. Finally, if one takes the relations of contrariety and subcontrariety to be logically on a par (and several authors have done so, for good reasons), then the equal-sized tetrahedra in RDH achieve greater congruence; however, if one takes contrariety to be a more important logical relation than subcontrariety (and several authors have done so, for equally good reasons), then the large/small tetrahedra in NTH fare better.

Our overall conclusion, then, is that RDH and NTH are *both* useful visualizations of $\mathbb{B}_4$; whichever one is ultimately adopted will depend on which logical properties of $\mathbb{B}_4$ the diagram author wants to highlight most prominently. Generally speaking, it seems that RDH allows one to visually emphasize the opposition relations obtaining in $\mathbb{B}_4$, whereas NTH more readily focuses on the visualization of its implication relations. These considerations should be taken into account by any researcher in artificial intelligence (and other fields) who makes use of $\mathbb{B}_4$, and wishes to clarify/illustrate her theorizing by means of an Aristotelian diagram.

Acknowledgements. A preliminary version of this paper was presented at the Diagrams 2016 conference in Philadelphia, PA, USA. We would like to thank the audience of that presentation, as well as Koen Roelandt, Margaux Smets and two anonymous reviewers of this journal for their useful feedback. The first author is financially supported by a Postdoctoral Fellowship of the Research Foundation–Flanders (FWO).

References

[1] L. Amgoud, P. Besnard, and A. Hunter. Foundations for a logic of arguments. In P. Cabalar, M. D. A. Herzig, and D. Pearce, editors, *Logical Reasoning and*

Computation: Essays dedicated to Luis Fariñas del Cerro, pages 95–107. IRIT, Toulouse, 2016.

[2] L. Amgoud and H. Prade. Can AI models capture natural language argumentation? *International Journal of Cognitive Informatics and Natural Intelligence*, 6(3):19–32, 2012.

[3] L. Amgoud and H. Prade. Towards a logic of argumentation. In E. Hüllermeier et al., editors, *Scalable Uncertainty Management 2012*, LNCS 7520, pages 558–565. Springer, Berlin, 2012.

[4] L. Amgoud and H. Prade. A formal concept view of formal argumentation. In L. C. van der Gaag, editor, *Symbolic and Quantiative Approaches to Resoning with Uncertainty (ECSQARU 2013)*, LNCS 7958, pages 1–12. Springer, Berlin, 2013.

[5] M. Barr and C. Wells. *Category Theory for Computing Science*. Prentice Hall, New York, NY, 1990.

[6] P. Bernhard. Visualizations of the square of opposition. *Logica Universalis*, 2:31–41, 2008.

[7] W. Carnielli and C. Pizzi. *Modalities and Multimodalities*. Springer, Dordrecht, 2008.

[8] L. Carroll. *Symbolic Logic. Edited, with annotations and an introduction by William Warren Bartley III*. Clarkson N. Potter, New York, NY, 1977.

[9] P. Chapman, G. Stapleton, P. Rodgers, L. Micallef, and A. Blake. Visualizing sets: An empirical comparison of diagram types. In T. Dwyer, H. Purchase, and A. Delaney, editors, *Diagrammatic Representation and Inference*, LNCS 8578, pages 146–160. Springer, Berlin, 2014.

[10] P. Cheng. Algebra diagrams: A HANDi introduction. In P. T. Cox, B. Plimmer, and P. Rodgers, editors, *Diagrammatic Representation and Inference*, LNCS 7352, pages 178–192. Springer, Berlin, 2012.

[11] D. Ciucci. Orthopairs in the 1960s: Historical remarks and new ideas. In C. Cornelis et al., editors, *Rough Sets and Current Trends in Computing (RSCTC 2014)*, LNCS 8536, pages 1–12. Springer, Berlin, 2014.

[12] D. Ciucci. Orthopairs and granular computing. *Granular Computing*, 1:159–170, 2016.

[13] D. Ciucci, D. Dubois, and H. Prade. Oppositions in rough set theory. In T. Li, H. S. Nguyen, G. Wang, J. Grzymala-Busse, R. Janicki, A. E. Hassanien, and H. Yu, editors, *Rough Sets and Knowledge Technology*, LNCS 7414, pages 504–513. Springer, Berlin, 2012.

[14] D. Ciucci, D. Dubois, and H. Prade. The structure of oppositions in rough set theory and formal concept analysis – toward a new bridge between the two settings. In C. Beierle and C. Meghini, editors, *Foundations of Information and Knowledge Systems (FoIKS 2014)*, LNCS 8367, pages 154–173. Springer, Berlin, 2014.

[15] D. Ciucci, D. Dubois, and H. Prade. Structures of opposition in fuzzy rough sets. *Fundamenta Informaticae*, 142:1–19, 2015.

[16] D. Ciucci, D. Dubois, and H. Prade. Structures of opposition induced by relations. The Boolean and the gradual cases. *Annals of Mathematics and Artificial Intelligence*, 76:351–373, 2016.

[17] L. Demey. Algebraic aspects of duality diagrams. In P. T. Cox, B. Plimmer, and P. Rodgers, editors, *Diagrammatic Representation and Inference*, LNCS 7352, pages 300–302. Springer, Berlin, 2012.

[18] L. Demey. Structures of oppositions for public announcement logic. In J.-Y. Béziau and D. Jacquette, editors, *Around and Beyond the Square of Opposition*, pages 313–339. Springer, Basel, 2012.

[19] L. Demey. Interactively illustrating the context-sensitivity of Aristotelian diagrams. In H. Christiansen, I. Stojanovic, and G. Papadopoulos, editors, *Modeling and Using Context*, LNCS 9405, pages 331–345. Springer, Berlin, 2015.

[20] L. Demey. Using syllogistics to teach metalogic. *Metaphilosophy*, 48:575–590, 2017.

[21] L. Demey. Aristotelian diagrams in the debate on future contingents. *Sophia*, DOI: 10.1007/s11841-017-0632-7, 2018.

[22] L. Demey. The logical geometry of the cube of opposition in knowledge representation. Manuscript.

[23] L. Demey and H. Smessaert. Logische geometrie en pragmatiek. In F. Van De Velde, H. Smessaert, F. Van Eynde, and S. Verbrugge, editors, *Patroon en argument*, pages 553–564. Leuven University Press, Leuven, 2014.

[24] L. Demey and H. Smessaert. The relationship between Aristotelian and Hasse diagrams. In T. Dwyer, H. Purchase, and A. Delaney, editors, *Diagrammatic Representation and Inference*, LNCS 8578, pages 213–227. Springer, Berlin, 2014.

[25] L. Demey and H. Smessaert. The interaction between logic and geometry in Aristotelian diagrams. In M. Jamnik, Y. Uesaka, and S. Elzer Schwartz, editors, *Diagrammatic Representation and Inference*, LNCS 9781, pages 67–82. Springer, Berlin, 2016.

[26] L. Demey and H. Smessaert. Metalogical decorations of logical diagrams. *Logica Universalis*, 10:233–292, 2016.

[27] L. Demey and H. Smessaert. Shape heuristics in Aristotelian diagrams. In O. Kutz, S. Borgo, and M. Bhatt, editors, *Shapes 3.0 Proceedings*, Workshop Proceedings 1616, pages 35–45. CEUR, Aachen, 2016.

[28] L. Demey and H. Smessaert. Logical and geometrical distance in polyhedral Aristotelian diagrams in knowledge representation. *Symmetry*, 9(10):204, 2017.

[29] L. Demey and H. Smessaert. Aristotelian and duality relations beyond the square of opposition. In P. Chapman, G. Stapleton, A. Moktefi, S. Perez-Kriz, and F. Bellucci, editors, *Diagrammatic Representation and Inference*, LNCS 10871. Springer, Berlin, 2018.

[30] L. Demey and H. Smessaert. Combinatorial bitstring semantics for arbitrary logical fragments. *Journal of Philosophical Logic*, 47:325–363, 2018.

[31] L. Demey and P. Steinkrüger. De logische geometrie van Johannes Buridanus' modale achthoek. *Tijdschrift voor Filosofie*, 79:217–238, 2017.

[32] M. M. Deza and E. Deza. *Encyclopedia of Distances*. Springer, Dordrecht, 2009.

[33] D. Dubois and H. Prade. From Blanché's hexagonal organization of concepts to formal concept analysis and possibility theory. *Logica Universalis*, 6:149–169, 2012.

[34] D. Dubois and H. Prade. Formal concept analysis from the standpoint of possibility theory. In J. Baixeries, C. Sacarea, and M. Ojeda-Aciego, editors, *Formal Concept Analysis (ICFCA 2015)*, LNCS 9113, pages 21–38. Springer, Berlin, 2015.

[35] D. Dubois and H. Prade. Gradual structures of oppositions. In L. Magdalena, J. L. Verdegay, and F. Esteva, editors, *Enric Trillas: A Passion for Fuzzy Sets*, SFSC 322, pages 79–91. Springer, Berlin, 2015.

[36] D. Dubois, H. Prade, and A. Rico. The cube of opposition – a structure underlying many knowledge representation formalisms. In Q. Yang and M. Wooldridge, editors, *Proceedings of the Twenty-Fourth International Joint Conference on Artificial Intelligence (IJCAI 2015)*, pages 2933–2939. AAAI Press, Palo Alto, CA, 2015.

[37] D. Dubois, H. Prade, and A. Rico. The cube of opposition and the complete appraisal of situations by means of Sugeno integrals. In F. Esposito et al., editors, *Foundations of Intelligent Systems (ISMIS 2015)*, LNCS 9384, pages 197–207. Springer, Berlin, 2015.

[38] D. Dubois, H. Prade, and A. Rico. Graded cubes of opposition and possibility theory with fuzzy events. *International Journal of Approximate Reasoning*, 84:168–185, 2017.

[39] D. Dubois, H. Prade, and A. Rico. Organizing families of aggregation operators into a cube of opposition. In J. Kacprzyk, D. Filev, and G. Beliakov, editors, *Granular, Soft and Fuzzy Approaches for Intelligent Systems*, pages 27–45. Springer, Berlin, 2017.

[40] A. Fish and J. Flower. Euler diagram decomposition. In G. Stapleton, J. Howse, and J. Lee, editors, *Diagrammatic Representation and Inference*, LNCS 5223, pages 28–44. Springer, Berlin, 2008.

[41] A. Fish, B. Khazaei, and C. Roast. User-comprehension of Euler diagrams. *Journal of Visual Languages and Computing*, 22:340–354, 2011.

[42] M. Fitting and R. L. Mendelsohn. *First-Order Modal Logic*. Kluwer, Dordrecht, 1998.

[43] J. Flower, G. Stapleton, and P. Rodgers. On the drawability of 3D Venn and Euler diagrams. *Journal of Visual Languages and Computing*, 25:186–209, 2014.

[44] J. D. García-Cruz. The hypercube of dynamic opposition. In J.-Y. Béziau, A. Buchsbaum, and M. Correia, editors, *5th World Congress on the Square of Opposition*, pages 25–27, Santiago, 2016. Pontificia Universidad Católica de Chile.

[45] A. Gilio, N. Pfeifer, and G. Sanfilippo. Transitivity in coherence-based probability logic. *Journal of Applied Logic*, 14:46–64, 2016.

[46] S. Givant and P. Halmos. *Introduction to Boolean Algebras*. Springer, New York, NY, 2009.

[47] I. Glöckner. *Fuzzy Quantifiers*. Springer, Berlin, 2006.

[48] B. Gottfried. The diamond of contraries. *Journal of Visual Languages and Computing*, 26:29–41, 2015.

[49] C. Gurr. Effective diagrammatic communication: Syntactic, semantic and pragmatic issues. *Journal of Visual Languages and Computing*, 10:317–342, 1999.

[50] I. Her. Description of the f.c.c. lattice geometry through a four-dimensional hypercube. *Acta Crystallographica A*, 51:659–662, 1995.

[51] L. R. Horn. *A Natural History of Negation*. University of Chicago Press, Chicago, IL, 1989.

[52] G. E. Hughes. The modal logic of John Buridan. In G. Corsi, C. Mangione, and M. Mugnai, editors, *Atti del convegno internazionale di storia della logica, le teorie delle modalità*, pages 93–111. CLUEB, 1987.

[53] P. J. Hurley. *A Concise Introduction to Logic (11th ed.)*. Wadsworth, Boston, MA, 2012.

[54] L. H. Kauffman. The mathematics of Charles Sanders Peirce. *Cybernetics & Human Knowing*, 8:79–110, 2001.

[55] G. Klima, editor. *John Buridan, Summulae de Dialectica*. Yale University Press, 2001.

[56] J. Larkin and H. Simon. Why a diagram is (sometimes) worth ten thousand words. *Cognitive Science*, 11:65–99, 1987.

[57] W. Lenzen. How to square knowledge and belief. In J.-Y. Béziau and D. Jacquette, editors, *Around and Beyond the Square of Opposition*, pages 305–311. Springer, Basel, 2012.

[58] D. Luzeaux, J. Sallantin, and C. Dartnell. Logical extensions of Aristotle's square. *Logica Universalis*, 2:167–187, 2008.

[59] L. Miclet and H. Prade. Analogical proportions and square of oppositions. In A. Laurent et al., editors, *Information Processing and Management of Uncertainty in Knowledge-Based Systems 2014, Part II*, CCIS 442, pages 324–334. Springer, Berlin, 2014.

[60] A. Moretti. *The Geometry of Logical Opposition*. PhD thesis, University of Neuchâtel, 2009.

[61] A. Moretti. Was Lewis Carroll an amazing oppositional geometer? *History and Philosophy of Logic*, 35:383–409, 2014.

[62] P. Murinová and V. Novák. Analysis of generalized square of opposition with intermediate quantifiers. *Fuzzy Sets and Systems*, 242:89–113, 2014.

[63] P. Murinová and V. Novák. Graded generalized hexagon in fuzzy natural logic. In J. P. Carvalho et al., editors, *Information Processing and Management of Uncertainty in Knowledge-Based Systems 2016, Part II*, CCIS 611, pages 36–47. Springer, Berlin, 2016.

[64] P. Murinová and V. Novák. Syllogisms and 5-square of opposition with intermediate quantifiers in fuzzy natural logic. *Logica Universalis*, 10:339–357, 2016.

[65] B. Nagy. Reasoning by intervals. In D. Barker-Plummer, R. Cox, and N. Swoboda, editors, *Diagrammatic Representation and Inference*, LNCS 4045, pages 145–147. Springer, Berlin, 2006.

[66] B. Nagy and R. Strand. Non-traditional grids embedded in $\mathbb{Z}^n$. *International Journal of Shape Modeling*, 14:209–228, 2008.

[67] T. Parsons. The traditional square of opposition. In E. N. Zalta, editor, *Stanford Encyclopedia of Philosophy (Summer 2017 Edition)*. CSLI, Stanford, CA, 2017.

[68] R. Pellissier. Setting n-opposition. *Logica Universalis*, 2(2):235–263, 2008.

[69] P. Peterson. On the logic of "few", "many", and "most". *Notre Dame Journal of Formal Logic*, 20:155–179, 1979.

[70] N. Pfeifer and G. Sanfilippo. Probabilistic squares and hexagons of opposition under coherence. *International Journal of Approximate Reasoning*, 88:282–294, 2017.

[71] N. Pfeifer and G. Sanfilippo. Square of opposition under coherence. In M. B. Ferraro et al., editors, *Soft Methods for Data Science*, AISC 456, pages 407–414. Springer, Berlin, 2017.

[72] H. Prade and G. Richard. From analogical proportion to logical proportions. *Logica Universalis*, 7:441–505, 2013.

[73] H. Prade and G. Richard. Picking the one that does not fit – a matter of logical proportions. In G. Pasi, J. Montero, and D. Ciucci, editors, *Proceedings of the 8th conference of the European Society for Fuzzy Logic and Technology (EUSFLAT-13)*, pages 392–399. Atlantis Press, Amsterdam, 2013.

[74] H. Prade and G. Richard. On different ways to be (dis)similar to elements in a set. Boolean analysis and graded extension. In J. P. Carvalho et al., editors, *Information Processing and Management of Uncertainty in Knowledge-Based Systems 2016, Part II*, CCIS 611, pages 605–618. Springer, Berlin, 2016.

[75] H. Prade and G. Richard. From the structures of opposition between similarity and dissimilarity indicators to logical proportions. In G. Dodig-Crnkovic and R. Giovagnoli, editors, *Representation and Reality in Humans, Other Living Organisms and Intelligent Machines*, pages 279–299. Springer, Berlin, 2017.

[76] S. Read. John Buridan's theory of consequence and his octagons of opposition. In J.-Y. Béziau and D. Jacquette, editors, *Around and Beyond the Square of Opposition*, pages 93–110. Springer, 2012.

[77] R. M. Roth. *Introduction to Coding Theory*. Cambridge University Press, Cambridge, 2006.

[78] P. Sauriol. Remarques sur la théorie de l'hexagone logique de Blanché. *Dialogue*, 7:374–390, 1968.

[79] H. Slater. Back to Aristotle! *Logic and Logical Philosophy*, 21:275–283, 2011.

[80] H. Smessaert. On the 3D visualisation of logical relations. *Logica Universalis*, 3:303–332, 2009.

[81] H. Smessaert. Boolean differences between two hexagonal extensions of the logical square of oppositions. In P. T. Cox, B. Plimmer, and P. Rodgers, editors, *Diagrammatic Representation and Inference*, LNCS 7352, pages 193–199. Springer, Berlin, 2012.

[82] H. Smessaert and L. Demey. Logical and geometrical complementarities between Aristotelian diagrams. In T. Dwyer, H. Purchase, and A. Delaney, editors, *Diagrammatic Representation and Inference*, LNCS 8578, pages 246–260. Springer, Berlin, 2014.

[83] H. Smessaert and L. Demey. Logical geometries and information in the square of opposition. *Journal of Logic, Language and Information*, 23:527–565, 2014.

[84] H. Smessaert and L. Demey. Béziau's contributions to the logical geometry of modalities and quantifiers. In A. Koslow and A. Buchsbaum, editors, *The Road to Universal Logic*, pages 475–493. Springer, Basel, 2015.

[85] H. Smessaert and L. Demey. Visualising the Boolean algebra $\mathbb{B}_4$ in 3D. In M. Jamnik, Y. Uesaka, and S. Elzer Schwartz, editors, *Diagrammatic Representation and Inference*, LNCS 9781, pages 289–292. Springer, Berlin, 2016.

[86] H. Smessaert and L. Demey. The unreasonable effectiveness of bitstrings in logical geometry. In J.-Y. Béziau and G. Basti, editors, *The Square of Opposition: A Cornerstone of Thought*, pages 197–214. Springer, Basel, 2017.

[87] R. Strand. Weighted distances based on neighborhood sequences for point-lattices. *Discrete Applied Mathematics*, 157:641–652, 2009.

[88] R. Strand, B. Nagy, and G. Borgefors. Digital distance functions on three-dimensional grids. *Theoretical Computer Science*, 412:1350–1363, 2011.

[89] E. Trillas and R. Seising. Turning around the ideas of 'meaning' and 'complement'. In M. Collan, M. Fedrizzi, and J. Kacprzyk, editors, *Fuzzy Technology*, SFSC 335, pages 3–31. Springer, Berlin, 2016.

[90] B. Tversky. Prolegomenon to scientific visualizations. In J. K. Gilbert, editor, *Visualization in Science Education*, pages 29–42. Springer, Dordrecht, 2005.

[91] B. Tversky. Visualizing thought. *Topics in Cognitive Science*, 3:499–535, 2011.

[92] M. Urbas, M. Jamnik, G. Stapleton, and J. Flower. Speedith: A diagrammatic reasoner for spider diagrams. In P. T. Cox, B. Plimmer, and P. Rodgers, editors, *Diagrammatic Representation and Inference*, LNCS 7352, pages 163–177. Springer, Berlin, 2012.

[93] L. Čomić and B. Nagy. A topological 4-coordinate sytem for the face centered cubic grid. *Pattern Recognition Letters*, 83:67–74, 2016.

[94] Y. Yao. Duality in rough set theory based on the square of opposition. *Fundamenta Informaticae*, 127:49–64, 2013.

[95] X. Yue, Y. Chen, D. Miao, and J. Qian. Tri-partition neighborhood covering reduction for robust classification. *International Journal of Approximate Reasoning*, 83:371–384, 2017.

[96] S. Zellweger. Untapped potential in Peirce's iconic notation for the sixteen binary connectives. In N. Houser, D. D. Roberts, and J. Van Evra, editors, *Studies in the Logic of Charles Peirce*, pages 334–386. Indiana University Press, Bloomington, IN, 1997.